Virus Research 265 (2019) 104–114

Contents lists available at ScienceDirect

Virus Research

journal homepage: www.elsevier.com/locate/virusres

Characteristics of enterovirus 71-induced cell death and genome scanning to identify viral genes involved in virus-induced cell apoptosis

Jinjin Bai[a], Xixi Chen[a], Qingqing Liu[b], Xin Zhou[a], Jian-Er Long[a,b,*]

[a] Key Laboratory of Medical Molecular Virology of Ministries of Education and Health, Shanghai Medical College of Fudan University, Shanghai 200032, China
[b] Laboratory of Medical Microbiology, Department of Medical Microbiology and Parasitology, Shanghai Medical College of Fudan University, 138 Yixueyuan R., Shanghai 200032, China

ARTICLE INFO

Keywords:
Nterovirus 71
Programmed cell death
Apoptosis
Genome scanning

ABSTRACT

Enterovirus 71 (EV71) causes hand-foot-and-mouth disease and severe neural complications in infants and young children. Viral pathogenesis is associated with virus-induced cell death and inflammatory cytokine production, which is usually correlated with the type of programmed cell death. EV71-infected cells were analyzed through microscopy, cell staining, and immunoblotting to determine the characteristics of EV71-induced cell death. Results demonstrated that EV71 infection induced cell shrinkage, nuclear condensation, decreased mitochondrial potential, and membrane phosphatidylserine translocation. Caspase-9 activation, poly (ADP-ribose) polymerase cleavage, and lactate dehydrogenase release were also observed during virus-induced cell death. The activated gasdermin D (GSDMD) and the phosphorylated mixed lineage kinase domain-like protein (p-MLKL) were not detected. These observations indicated that EV71-induced cell death was mainly executed by apoptosis through the intrinsic pathway rather than by GSDMD-mediated pyroptosis and p-MLKL-mediated necroptosis. Genome scanning analysis identified that EV71 2A, 2B, and 3C might be the determinant genes of virus-induced cell death. Further experiments showed that EV71 2A- and 3C-induced cell death exhibited dependence on their protease activities but involved different mechanisms. EV71 2A-induced cell death was correlated with the shut-off of host cap-dependent translation, whereas EV71 3C-induced cell death might not be ascribed to this mechanism. These findings would enhance our understanding of EV71 infection and viral pathogenesis, and help identify antiviral targets.

1. Introduction

Enterovirus 71 (EV71) has been described as the major etiology of hand-foot-and-mouth disease (HFMD) in infants and young children. EV71 infections also cause nervous system complications and even lead to death (McMinn, 2012; Solomon et al., 2010; Xing et al., 2014). As a member of the family of *Picornavirus*, EV71 is a single- and positive-strand RNA virus with a genome size of approximately 7.4 kb. The viral genome encodes a long polyprotein that is cleaved to three proteins (P1, P2, and P3); they are finally hydrolyzed into four structural proteins (VP1-VP4) and seven nonstructural proteins (2A, 2B, 2C, 3A, 3B, 3C, and 3D), which are mainly processed by the viral protease, namely, EV71 2A and 3C (Solomon et al., 2010; Yuan et al., 2018). The two viral proteins are cysteine proteases that contribute to viral protein maturation and host factor regulation. Such regulations are correlated with viral replication, host cytokine and proinflammatory factor production, and cell death (Pathinayake et al., 2015; Yuan et al., 2018). However, the viral pathogenesis of EV71 infection is largely unknown.

Previous studies suggested that EV71-induced severe illness is associated with pro-inflammatory cytokine production and programmed cell death (PCD) (Bek and McMinn, 2012; Lee, 2016; Ong and Wong, 2015; Ooi et al., 2010; Weng et al., 2010). PCD plays an important role in host defense against pathogenic infections, proinflammatory responses, viral replication, and viral evasion of host immune responses (Chan et al., 2015; Kaiser et al., 2013; Lupfer et al., 2015; Nagata and Tanaka, 2017). Some viral infections can trigger programmed cell death through different pathways, including apoptosis, pyroptosis, and necroptosis. Apoptosis is considered a nonlytic and usually an immunologically silent form of cell death, whereas pyroptosis and necroptosis are programmed lytic cell death with inflammatory responses (Chan et al., 2015; Kaiser et al., 2013; Lupfer et al., 2015; Nagata and Tanaka, 2017).

* Corresponding author at: Key Laboratory of Medical Molecular Virology of Ministries of Education and Health, Shanghai Medical College of Fudan University, 138 Yixueyuan R., Shanghai 200032, China.
E-mail address: longjianer@fudan.edu.cn (J.-E. Long).

https://doi.org/10.1016/j.virusres.2019.03.017
Received 20 December 2018; Received in revised form 19 February 2019; Accepted 21 March 2019
Available online 22 March 2019
0168-1702/

Cell apoptosis can be triggered by intrinsic and extrinsic pathways. Intrinsic pathways are mainly mediated by the mitochondria, whereas extrinsic pathways are initiated by the recognition of tumor necrosis factor receptor or FAS-ligand receptors (Nagata and Tanaka, 2017; Orzalli and Kagan, 2017). Mitochondria play a major role in apoptosis. Upon activation by apoptotic signals, the mitochondrial membrane can be disrupted to release apoptosis-associated substances, including cytochrome c, resulting in the activation of many cysteine aspartate-specific proteases (caspase). Caspases are key regulatory and effecter proteins during apoptosis. In the intrinsic pathway, pro-caspase-9 is cleaved and activated, thereby activating caspase-3. In the extrinsic pathway, caspase-8 is activated by a cascade of responses to extracellular death signals, further activating caspase-3 (Nagata and Tanaka, 2017). The activated caspase-3 results in the proteolysis of many target proteins, including poly ADP-ribose polymerase (PARP), which is a DNA-repairing enzyme. These events further trigger an apoptotic process with various characteristics, including cellular shrinkage, nuclear condensation, and membrane blebbing (Chan et al., 2015; Nagata and Tanaka, 2017). However, pyroptosis is mainly mediated by inflammatory caspases (caspase-1, caspase-4, caspase-5, and caspase-11), which cleave gasdermin D (GSDMD) within a linker between its N- and C-terminal domains. The released gasdermin-N domain binds to phosphoinositides in the plasma membrane and oligomerizes to generate membrane pores, which allow the release of IL-1β and IL-18 (Ding et al., 2016; Kovacs and Miao, 2017; Place and Kanneganti, 2017; Shi et al., 2015, 2017). As an alternative cell death pathway, necroptosis is mainly mediated by receptor-interacting protein kinases and the mixed lineage kinase domain-like protein (MLKL). Phosphorylated MLKL is an effecter protein that oligomerizes to form membrane pores and causes lytic cell death (Cai et al., 2014; Kaczmarek et al., 2013; Murphy et al., 2013; Pasparakis and Vandenabeele, 2015). Pyroptosis and necroptosis are characterized by the rupture of the cell membrane and the release of danger-associated molecular patterns, including cellular enzymes and high-inflammatory cytokines (Cai et al., 2014; Kaczmarek et al., 2013; Murphy et al., 2013; Pasparakis and Vandenabeele, 2015).

EV71 infection induces cell apoptosis. Several viral proteins, including EV71 2A, 2B, and 3C, play a role in apoptotic processes (Cong et al., 2016; Han and Cong, 2017; Kuo et al., 2002; Li et al., 2017, 2002). EV71 infection increases IL-1β and IL-18 production and activates AIM 2- and NLRP3-inflammasomes, which are correlated with EV71 2A, 3C, and 3D (Wang et al., 2015, 2017b; Wang et al., 2018; Yogarajah et al., 2017). These results suggested that EV71 infection possibly induces cell pyroptosis. However, Lei et al (Lei et al., 2017) reported that EV71 3C cleaves GSDMD at Q193-G194, resulting in a dysfunctional N-terminal and inhibiting virus-induced pyroptosis *in vitro*. EV71-induced cell death is dependent on viral genome replication and protein synthesis (Shih et al., 2008). Determinant genes in EV71 genome involved in virus-induced cell death should be systematically studied, and the characteristics of virus-induced cell death should be further clarified. In the present study, the characteristic of EV71-induced cell death was determined through microscopy, cell staining, and immunoblotting of some key host factors during cell apoptosis, pyroptosis, and necroptosis. Our findings showed that EV71-induced cell death was mainly ascribed to apoptosis through the intrinsic pathway. Genome scanning analysis indicated that virus-induced apoptosis was mainly mediated by EV71 2A, 2B, and 3C. Further experiments revealed that EV71 2A- and 3C-induced cell apoptosis depended on protease activities *via* different mechanisms.

2. Materials and methods

2.1. Virus strain, cell lines, and reagents

EV71 strain (GenBank accession No. HQ891927, 064-Shanghai) was isolated from a patient with HFMD as previously described (Yan et al., 2012). Rhabdomyosarcoma (RD), HeLa, HEK293FT, and SH-SY5Y (brain tissue with neuroblastoma) cell lines were obtained from ATCC and cultured in DMEM (Gibco) supplemented with 10% fetal bovine serum (FBS). Secondary antibodies and mouse monoclonal antibodies against human caspase-3 (#9665), caspase-9 (#9502), PARP (#9542), MLKL (#14993), p-MLKL (#91689), STAT3α (#8768), and β-actin (#3700) were obtained from Cell Signaling Technology Inc. Mouse monoclonal antibody against EV71 VP1 (MAB1225-M05) and human GASDMD (ab210070) were purchased from Abnova. A tetraethylbenzimidazolylcarbocyanine iodide (JC-1) mitochondrial membrane potential assay kit was procured from Abcam. A lactate dehydrogenase (LDH) assay kit was bought from Promega. Staurosporine and z-VAD-fmk (z-VAD) were obtained from Med Chem Express. An IRES-guided RFP expression plasmid (pMSCV-IRES-mCherry FP) was a gift from Prof. Dario Vignali (Addgene plasmid # 52114).

2.2. Cell morphology and microscopy

RD and SH-SY5Y cells were seeded and infected with EV71 (MOI = 10 PFU/cell) for observation under microscopy to identify the morphological characteristics of EV71-infected cells. RD cells were also infected at an MOI of 1.0 and fixed with methanol at 6 h post-infection (hpi). The fixed cells were sequentially stained not only with monoclonal antibodies against VP1 and STAT3α but also with DAPI to observe the nuclear alteration. STAT3α was stained with the rabbit monoclonal antibody against human STAT3α, and the antibody against rabbit IgG was conjugated with Alexa Fluor™488 fluorescence dye. EV71 VP1 was stained with the mouse monoclonal antibody against EV71 VP1, and the goat anti-mouse IgG-Dye-light 594 was conjugated. Images were captured using a confocal laser scanning microscope (LeicaTCS SP5, GRE). RD cells were also stained with JC-1 to check the mitochondrial potential alteration after the cells were infected with the virus at the indicated time points. Images were captured with an EVOS F1 fluorescence microscope (Advanced Microscopy Group, USA).

2.3. Immunoblotting

The cells were harvested and lysed on ice by RIPA buffer supplemented with protease and phosphatase inhibitors, including PMSF, leupeptin, and aprotinin. Western blot was performed by utilizing the primary antibodies at indicated dilutions in accordance with the manufacturer's instructions. Anti-mouse IgG-HRP was diluted at 1:5000, and signals were visualized through chemiluminesence by using an ECL kit (Amersham Bioscience). The antibody against β-actin that functioned as loading and internal control was mixed with the antibodies against the target proteins to avoid the significant deviation of experimental manipulations. The same downstream manipulations were performed when the corresponding target protein was detected.

2.4. Cell staining and fluorescence-activated cell sorting (FACS) quantitative assay

RD or SH-SY5Y cells were infected with EV71 at an MOI of 1.0 and further incubated for another 16 h. Then, the cells were trypsinized and stained with propidium iodide (PI) and annexin V-FITC by using an annexin V-FITC/PI apoptosis detection kit (Shanghai YEASEN Biotech. Inc.) in accordance with the manufacturer's instructions. The stained cells were observed under a florescence microscope. For the FACS quantitative assay, the cells were pretreated with 20 μM z-VAD for 1 h or mock treated and then infected with EV71 at an MOI of 1.0. At the indicated time points, the cells were trypsinized and stained with PI and annexin V-FITC. FITC green fluorescence was quantified by FL1 channel (488 nm), and PI red fluorescence was detected by FL2 (535 nm).

2.5. LDH release assay

RD or SH-SY5Y cells were seeded in a 96-well plate and treated with

z-VAD at 20 μM for 1 h or mock treated and then infected with EV71 at an MOI of 1.0. At the indicated post-infection time points, the culture supernatant was collected for LDH assay. LDH release was detected with the LDH assay kit in accordance with the manual (Promega). LDH released from HeLa cells was analyzed similar to RD and SH-SY5Y cells, but the cells were infected with EV71 at MOI of 10.

2.6. Construction of plasmids for EV71 gene expression

Each cDNA of EV71 genes was cloned into the high-expression lentivirus vector pCDH-puro (System Bioscience, CD510B-1). Lentivirus particles were produced, and stable RD cells integrated with the lentivirus vectors were selected with puromycin in accordance with the manufacture's introductions. Control stable RD cell lines integrated with the control lentivirus vector pCDH-puro were simultaneously produced. Triple FLAG tags were fused followed by 2A and 3C genes in pCDH-2A or -3C plasmids. Both mutants with deleted proteases were also constructed. EV71 2A gene were mutated at C110A (code from TGC to GCC), and EV71 3A gene were mutated at H40D (code from GAC to GAT) (Cui et al., 2011; Mu et al., 2013).

2.7. Quantitative RT-PCR assay

The EV71 gene expression in cells was determined through quantitative RT-PCR (Q-PCR). In brief, 1.0 μg of denatured RNA was reverse transcribed with a random primer in a total volume of 10 μL. After incubation at 42 °C for 45 min, M-MLV reverse transcriptase was inactivated. EV71 gene was amplified with specific primers (Table S1) by running the following program: 95 °C for 4 min, followed by 40 cycles of 95 °C for 5 s, and 60 °C for 10 s. Fluorescence signals were acquired with a PCR machine (Applied Biosystems 9700, USA), and *Ct* was calculated with the supplied software. The β-actin gene was simultaneously detected as a reference control. The Δ*Ct* (average *Ct* – average *Ct* of the control) was calculated for fold alteration analysis. In this analysis, the fold change in each EV71 gene after transfection was calculated as $2PP^{-\Delta\Delta Ct}PP$. Each sample was quantified at least thrice and expressed as mean ± SD.

2.8. MTT assay for cellular viability detection

Cellular viability after EV71 gene transfection was determined by the MTT assay. In this procedure, 293FT or RD cells were seeded at $2 \times 10PP^4$ cells/well in 96-well plates for 16 h and then transfected with 200 ng/well plasmid of EV71 gene with Lipofectamine 2000 (Invitrogen) in a 96-well plate. The cells were further incubated for 72 h, and MTT and DMSO were added sequentially as previously described (Bian et al., 2015). The OD_{570nm} value was measured, and cell survival viability after transfection was expressed as $OD_{EV71gene\text{-}tranfected}/OD_{cell\ control} \times 100\%$.

2.9. Statistical analysis

Statistical analyses were performed in SPSS 16.0. Student's *t*-test was applied to the two groups of datasets. Statistical significance was considered at $P < 0.05$.

3. Results

3.1. Cell morphology and characteristics of EV71-induced cell death

EV71 infection induces remarkable cytopathic effects and finally leads to cell death. RD and neural SH-SY5Y cells were infected with EV71 to identify the characteristics of virus-induced cell death, and the morphological characteristics of the cells were observed at 16 hpi under light microscopy. The results showed that most infected cell became small and round and shrank (black arrows in Fig. 1A). However, several cells became swollen, round, and prone to rupture (indicated with red arrows in Fig. 1A). After the virus-infected RD cells were stained with antibodies against EV71 VP1 (red in Fig. 1B) and a constitutively-expressed protein STAT3α (green in Fig. 1B to outline the whole cell morphology), EV71-infected cells showed dramatically nuclear condensation and abnormality. The mitochondrial integrity of infected cells was also observed by staining with JC-1, a dye to detect the mitochondrial membrane potential, whose alteration is considered as an early marker of cell apoptosis(Huang et al., 2007). The results showed that EV71 infection led to JC-1 yielding green fluorescence, suggesting that EV71 infection decreased the cellular mitochondrial potential, thereby disrupting mitochondrial integrity (Fig. 1C). The infected cells were also stained with annexin V-FITC and PI at 16 hpi. Annexin V had a high affinity to cellular membrane phosphatidylserine (PS) (Eray et al., 2001), and once PS flipped from the inner face of the plasma membrane to the cell surface, PS could be stained with annexin V-FITC and implicated as an early marker of cell apoptosis (green in Fig. 1D). However, PI could stain nuclear DNA in the necrotic cells (red in Fig. 1D). The results of annexin V-FITC/PI double staining indicated that EV71 infection induced PS translocation and cell necrosis (Fig. 1D). These results also indicated that EV71-induced cell death exhibited markedly apoptotic characteristics and possibly involved other programmed cell death pathways, considering that the different cell morphological features were observed after the viral infection.

3.2. EV71 infection induced the caspase activation and PARP cleavage

EV71-induced cell death presented comprehensive characteristics, which indicated that several pathways were possibly contributed to the virus-induced cell death. Some caspases and their target proteins, such as caspase-3, caspase-8, caspase-9, and PARP, in RD and SH-SH5Y cells were determined after they were infected with EV71. The results showed that procapase-9 and procaspase-3 activation were detected at the late infection phase in the two cell lines (Fig. 2A and 2B). As a target of caspases, PARP is involved in the DNA repair, genomic stability, and programmed cell death. PARP cleavage is also considered an important molecular event of cell apoptosis (Oliver et al., 1998). In EV71-infected cells, the cleavage of a 116 kDa PARP was detected in SH-SY5Y and RD cells (Fig. 2C). However, procaspase-8 activation was undetectable in the two cell lines after the viral infection (data not shown). Caspase-9 is an initial caspase that mediates the mitochondrial apoptotic pathway (intrinsic apoptotic pathway), whereas caspase-8 is the initial caspase in the external apoptotic pathway (Nagata and Tanaka, 2017). These results suggested that EV71-induced cell death was mainly mediated by the intrinsic apoptotic pathway. To further identify whether pyroptosis and necroptosis were involved in viral infection, we detected the expression of GSDMD and MLKL. EV71 infection had not obviously altered GSDMD and MLKL levels. Their activated forms, namely, N-terminal GSDMD fragment and phosphorylated MLKL, were also not detected in RD, SH-SY5Y, and HeLa cells (Fig. S1). Therefore, EV71 infection might not induce GSDMD-mediated pyroptosis and p-MLKL-mediated necroptosis *in vitro*.

3.3. Caspase inhibitor inhibited EV71-induced cell death

RD and SH-SY5Y cells were pretreated with z-VAD (a pan-caspase inhibitor) and infected with EV71 to further understand the dynamics and characteristics of EV71-induced cell death. Then, the cells were stained with Annex V–FITC/PI and quantified via the FACS assay at the indicated time points. The virus-infected cells showed Annex V–FITC- and PI-positive staining (Fig. 1D), suggesting that the infected cells underwent apparent apoptosis and finally died. With the viral infection, the number of living cells (double negative cells in Figs. S2 and 3A) in both groups of pretreated with z-VAD and without treatment was decreased. However, the decrease was slowed down when the cells were pretreated with z-VAD (Figs. S2, 3A, and 3B). This observation implied

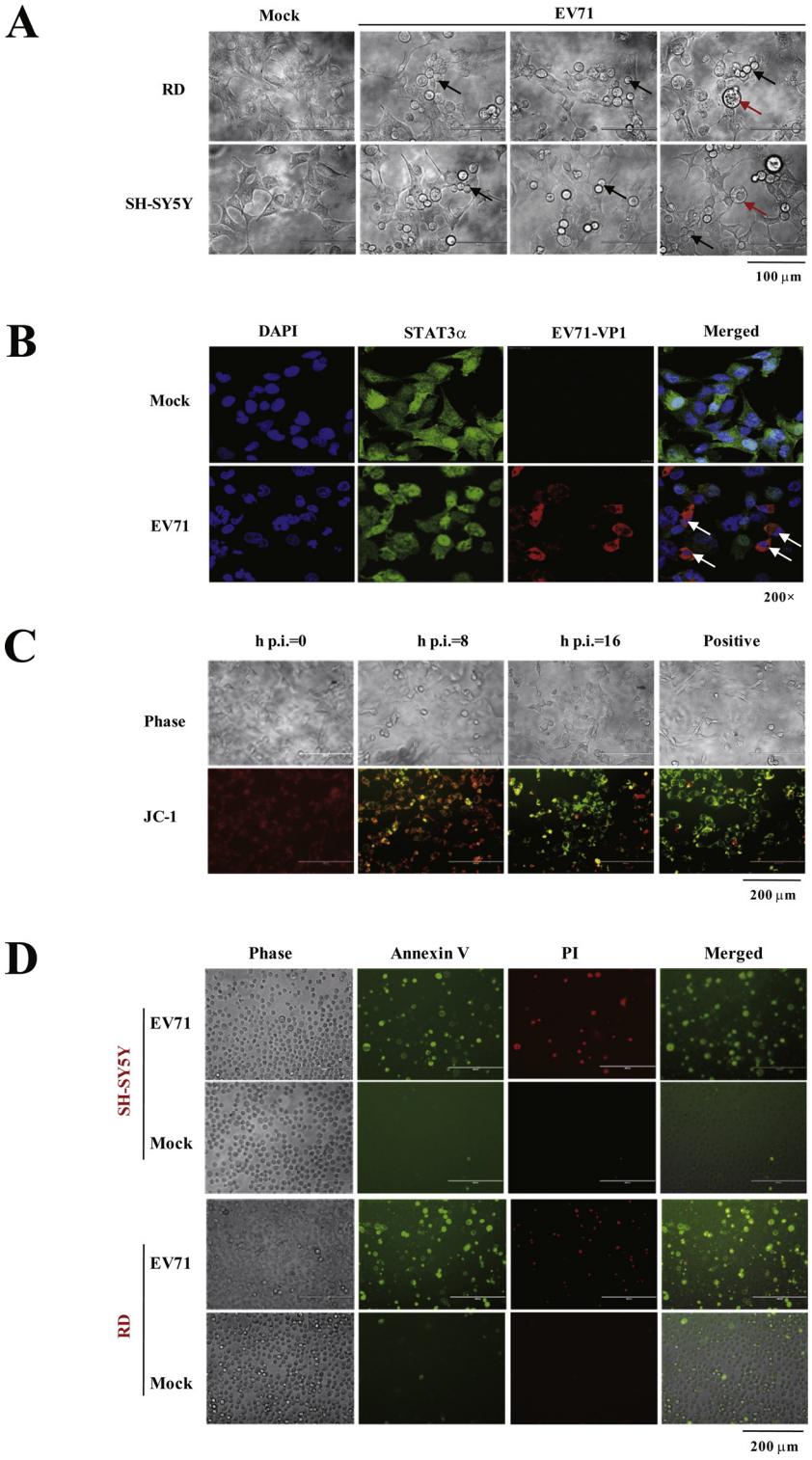

Fig. 1. Morphological characteristics of cells infected with EV71. (A) Morphological characteristics of RD and SH-SY5Y cells with EV71 infection (MOI = 10 at 16 hpi). (B) Confocal microscopy showing the abnormal nucleus in RD cells infected with EV71. The cells were infected with EV71 at an MOI of 1.0 for 6 h or mock treated, respectively subjected to immunofluorescence staining with monoclonal antibodies against human STAT3α (green) and EV71 VP1 (red), and stained with DAPI (blue). (C) JC-1 staining of RD cells infected with EV71 at indicated time points (MOI = 10). The cells treated with 1.0 μM staurosporine for 3 h were set as positive control. (D) Cell staining with PI and annexin V-FITC. RD and SH-SY5Y cells were infected with EV71 at an MOI of 1.0 for 16 h. The cells were then trypsinized for staining.

that EV71-induced cell death was a caspase activity-dependent process. LDH is a cellular enzyme that can be released into culture media from damaged cells and considered a biomarker for the integrity of cellular membrane and cytolysis. Similarly, we observed that LDH release was evidently induced at the late phase of EV71 infection in SH-SY5Y, RD, and HeLa cells. LDH release was also significantly inhibited by the pretreatment with z-VAD (Fig. 3C and 3D). This result indicated that the cell death induced by EV71 infection was dependent on caspase activity. To confirm this conclusion, we detected caspase-9 activation and PARP cleavage in SH-SY5Y and HeLa cells after they were infected with the virus. The results showed that the EV71-infected cells induced procaspase-9 activation and increased PARP cleavage, which was inhibited by z-VAD pretreatment (Fig. 4A and 4B). Combining the data collected from virus-infected cells pretreated with z-VAD and our other findings, we concluded that EV71 infection induced cell apoptosis and necrosis, which were correlated with caspase activation, and could be inhibited by caspase inhibitor.

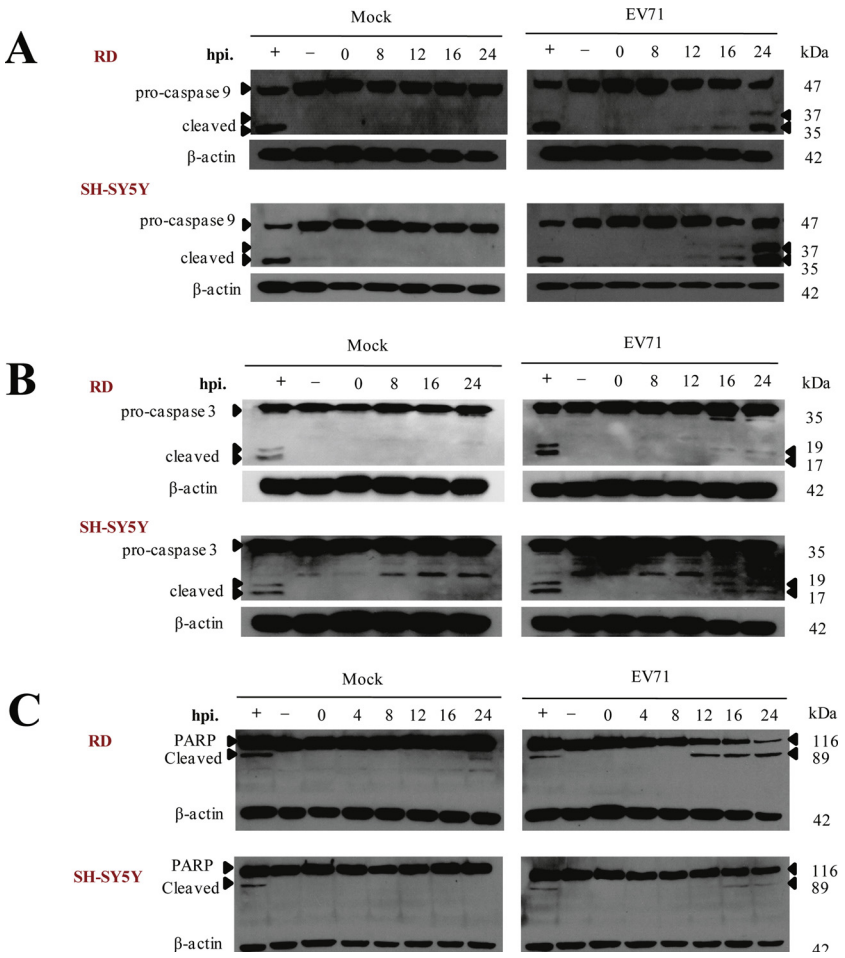

Fig. 2. EV71 infection induces caspase activation and PARP cleavage. (A) Caspase-9 activation induced by EV71 infection in RD and SH-SY5Y cells. The cells were infected with EV71 at an MOI of 1.0 and then collected for immunoblotting at the indicated time points. (B) Caspase-3 cleavage induced by EV71 infection in cells. The cells were infected and treated as Panel **A**. (C) The cleavage of PARP, which is a molecular target of caspases, was induced by EV71 infection in the cells. RD and SH-SY5Y cells were infected with EV71 and treated as Panel **A**. The cells treated with staurosporine at 1.0 μM for 3 h were considered as positve control. "+" and "-" symbols indicate the positive control and the mock-treated control, respectively.

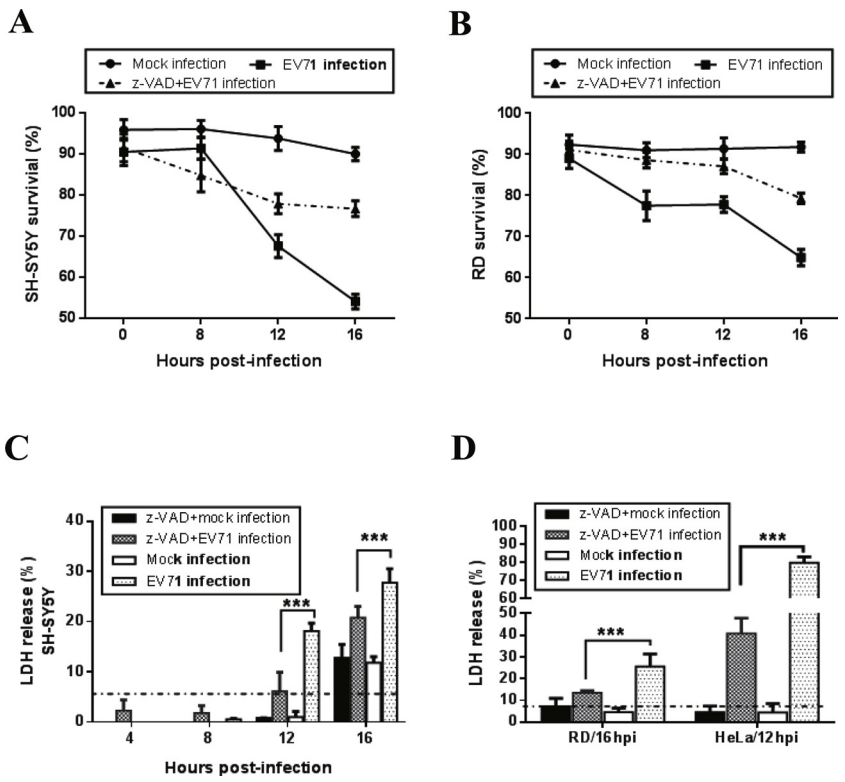

Fig. 3. EV71-induced cell apoptosis and LDH release were inhibited by a caspase inhibitor. Plot of the survival cells after EV71 infection with SH-SY5Y **(A)** and RD cells **(B)** by FACS assay. The cells were pretreatment with 20 μM z-VAD for 1 h or mock treated, and infected by EV71 at an MOI of 1.0. The infected cells were trypsinized for staining with annexin V-FITC and PI at the indicated time points. FACS experiments were repeated, and data were presented as mean ± SD. **(C)** Relative LDH release from SH-SY5Y cells, and **(D)** from RD and HeLa cells after EV71 infection. The cells were pretreated with 20 μM z-VAD for 1 h or mock treated. SH-SY5Y and RD cells were then infected with EV71 at an MOI of 1.0, but HeLa cells were infected at an MOI of 10. The culture media were collected from the cells at the indicated time points for LDH assay. $^{*}P < 0.05$, $^{**}P < 0.01$, and $^{***}P < 0.001$.

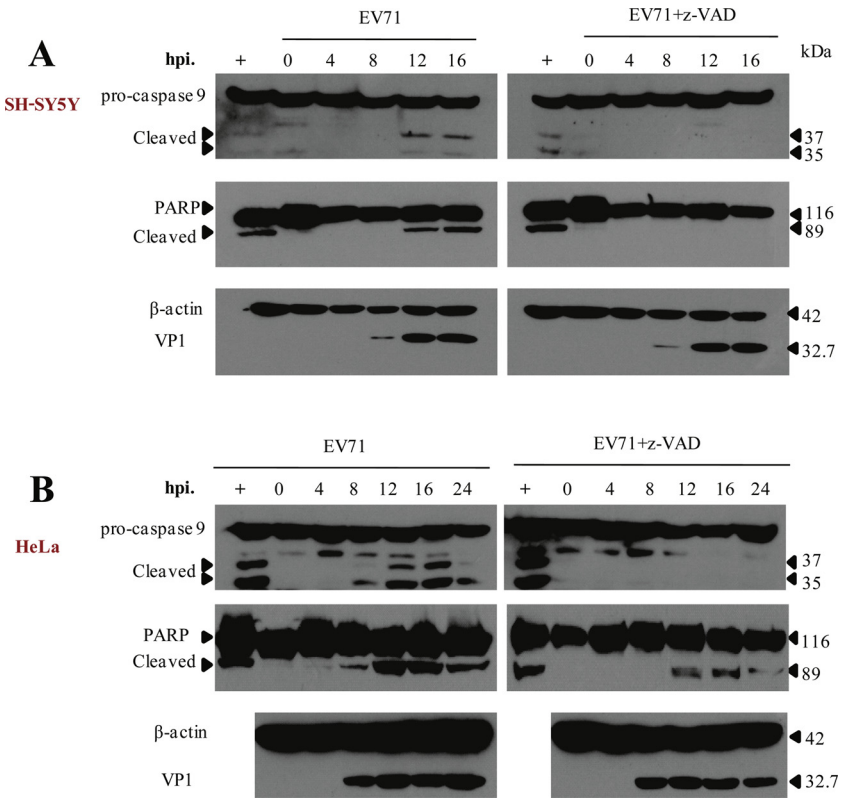

Fig. 4. PARP cleavage and caspase-9 activation induced by EV71 infection were inhibited by a caspase inhibitor. **(A)** Caspase-9 activation, PARP cleavage, and viral protein VP1 were detected after SH-SY5Y cells were infected with EV71. The cells were pretreatment with 20 μM z-VAD for 1 h or mock treated, and then infected by EV71 at an MOI of 1.0. The infected cells were collected for immunoblotting at the indicated time points. **(B)** Caspase-9 activation, PARP cleavage, and VP1 expression in HeLa cells were detected after they were infected with EV71. The cells were infected at an MOI of 10 and pretreated with z-VAD as Panel **A**. Cells treated with staurosporine were considered as the positve control of immunoblotting and indicated by "+".

3.4. Genome scanning to identify the genetic determinants in EV71-induced cell death

EV71 infection induces the cell apoptosis and necrosis, but the viral gene mainly involved in this process is unknown. In this study, genome scanning analysis was performed to identify the genetic determinant in the viral genome. Sixteen of functional gene fragments that covered the full-length genome of EV71, were included in this genome scanning and cloned into an overexpressing lentiviral plasmid named pCDH-puro (Fig. 5A). These constructions were confirmed by PCR and DNA sequencing (Fig. 5B). Then, lentiviral plasmids were applied to produce the lentiviral particles and further infect RD cells. Stable RD cells integrated with lentiviruses were selected with puromycin. The EV71 gene expression levels in stable RD cells were quantified by standard Q-PCR (Fig. 5C) except 2A. The cells integrated with pCDH-2A-puro were unavailable because the cells were dead after puromycin selection was performed. Consequently, the EV71 2A expression in RD cells was detected from the cells transfected with pCDH-2A-puro at 72 h post-transfection (close boxed in Fig. 5C). The Q-PCR results showed that all of the cloned genes were expressed in the cells. Then, these constructions were transfected into 293FT and RD cells. The cell viability after transfection was detected with the MTT assay, and the results demonstrated that transfection with EV71 2A or 3C gene in 293FT cells significantly induced cell death. Transfection with EV71 2A or 2B gene in RD cells had similar effects. Moreover, 3D and 3CD manifested weak effects that induced cell death (Fig. 5D).

3.5. EV71 2A- and 3C-induced cell death dependent on their protease activity

Genome scanning analysis revealed that EV71 2A and 3C have important roles in virus-induced cell death. EV71 2A and 3C participate in viral protein processing, serve as key regulators of host protein translation, and escape from immune responses through their protease activity (Yuan et al., 2018). The wild-type and mutated 2A and 3C ($2A^{C110A}$ and $3C^{H40D}$), whose protease activity centers were destroyed, were re-cloned and tagged with triple FLAGs to detect whether EV71 2A- and 3C-induced cell death were dependent on their protease activity (Figs. 6A and 6B). EV71 2A and 3C expressions and their mutants were detected after transfecting these constructions into 293FT cells at 72 h post-transfection (Fig. 6C). Procaspase-9 activation and PARP cleavage were also analyzed by immunoblotting after the cells were transfected with EV71 2A and the mutant $2A^{C110A}$ at the indicated time points. The results showed that the activated caspase-9 and the cleaved PARP remarkably increased from 48 h to 96 h after being transfected with 2A, but not with the mutant $2A^{C110A}$ (Fig. 6D). These results indicated that the 2A-induced caspase-9 activation and PARP cleavage were dependent on the 2A protease activity. To further confirm this observation, we transfected EV71 2A, 3C, and their mutants to SH-SY5Y cells and determined caspase-9 activation and PARP cleavage at 72 and 96 h post-transfection. The results indicated that 2A and 3C induced caspase-9 activation and PARP cleavage, but the induction was dependent on protease activity (Fig. 6E). Furthermore, the survival viability of the cells tranfected with EV71 2A, 3C, and their mutant constructions were compared in 293FT and SH-SY5Y cells. The results showed that transfection with 2A and 3C significantly decreased the cell viability at 72 h post-transfection, but transfection with their protease mutants showed no apparent effects on the cell survival viability (Fig. 6F). These results indicated that 2A and 3C play essential roles in EV71-induced cell death in a protease activity-dependent manner.

3.6. EV71 2A and 3C induced cell death via different mechanisms

Considering that EV71 2A- and 3C-induced cell death depended on their protease activity, we further determined whether both viral proteases had a similar mechanism of cell death. Previous reports showed that EV71 2A and 3C result in the proteolysis of many host proteins and shutoff of host protein translation to benefit viral replication (Kuo et al., 2002; Yuan et al., 2018). If EV71 2A- and 3C-induced cell death was executed in the same way by shutting off cellular protein translation,

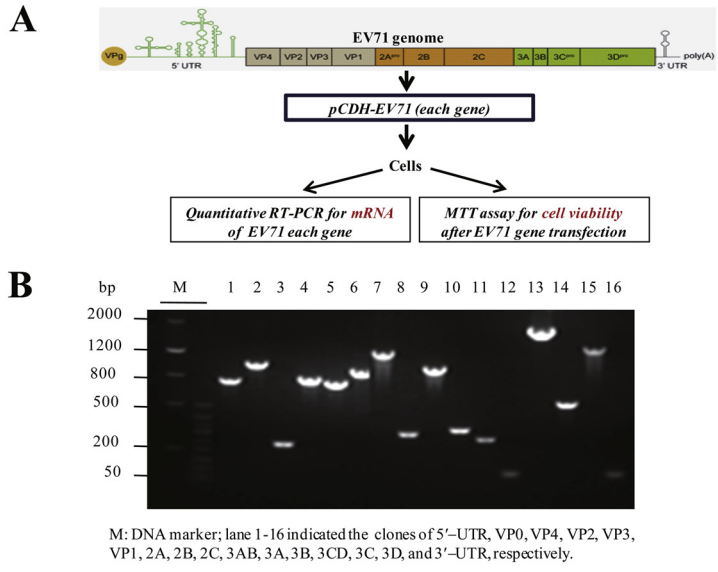

Fig. 5. Genome scanning to identify the genetic determinants in the EV71-induced cell death. (A) Flowchart of genome scanning to identify the viral determinants in the virus-induced cell death. **(B)** PCR to identify the clones of EV71 genes. Each EV71 gene was recombined into an overexpressing lentivirus plasmid. **(C)** Quantitative RT-PCR assay of EV71 mRNAs in stable RD cells. The cells were integrated with different EV71 genes in the recombinant lentivirus vectors. The recombinant lentivirus plasmids from Panel **B** were utilized to the package of the lentivirus particle, which were added to RD cells. The stable cell lines were then selected with puromycin. The cells stably integrated with the 2A gene were unavailable after puromycin selection was performed. The 2A close box indicated the data from the cells after transfection for 72 h with the 2A plasmid at 3.0 ug/well in a six-well plate. **(D)**. Relative cell survival viability after the cells were transfected with different EV71 genes. These plasmids overexpessing the EV71 genes were tranfected (200 ng/well in a 96-well plate) to 293FT or RD cells, and the cells were further incubated for 72 h. Cell survival viability was detected with the MTT assay. Each plasmid transfection was performed in quintuple in a 96-well plate, and the experiment was executed thrice. Data were shown mean ± SD. $^{*}P < 0.05$, $^{**}P < 0.01$, and $^{***}P < 0.001$.

host cap-dependent protein expression would be reduced by EV71 2A and 3C. To test this hypothesis, we co-transfected a housekeeping elongation factor 1α promoter-guided GFP-expressing plasmid and the plasmids overexpressing EV71 2A, 3C, $2A^{C110A}$, or $3C^{H40D}$ into SH-SY5Y cells. We then detected the effects of EV71 2A and 3C on the GFP expression. The results showed that the co-transfection with EV71 2A obviously inhibited the GFP expression, whereas the co-transfection with EV71 $2A^{C110A}$, 3C, or $3C^{H40D}$ did not have evident effects on the GFP expression (Fig. 7A). The results also suggested that EV71 2A-induced cell death was correlated with the shutoff of cellular cap-dependent protein translation in a protease activity-dependent manner, whereas EV71 3C was not the case. Further experiments involving the co-transfection of an IRES-guided red fluorescence cherry FP showed that the IRES-guided RFP expression was not evidently altered by EV71 2A, 3C, or their mutants (Fig. 7B). It indicated that viral 2A and 3C did not affect the viral IRES-guided protein translation. Consequently, EV71 2A-induced cell death was obviously different from that of EV71 3C, although the two viral proteases, which induced cell death, were dependent on their protease activities (Fig. 6).

4. Discussion

EV71 infection causes HFMD and severe neural complications in young children. The molecular pathogenesis of EV71 infection is correlated with virus-induced cell death and proinflammatory cytokines (Ooi et al., 2010; Solomon et al., 2010). Programmed cell death, including apoptosis, pyroptosis, and necroptosis, plays a significant role in inflammation and cytokine production. Apoptosis is considered nonlytic and immune silent, whereas pyroptosis and necroptosis are cell lytic and inflammatory through which cells usually show blebbing and disintegration of their membrane (Nagata and Tanaka, 2017; Orzalli and Kagan, 2017). Besides of neural and epithelial cells, RD and HeLa cells are widely-accepted cell models for the investigation of enteroviruses, including EV71, poliovirus, and Coxsackie viruses (Adeyemi et al., 2018; Fung et al., 2015; Wang et al., 2017a; Yang et al., 2018). More cell lines were utilized in our experiments to clarify

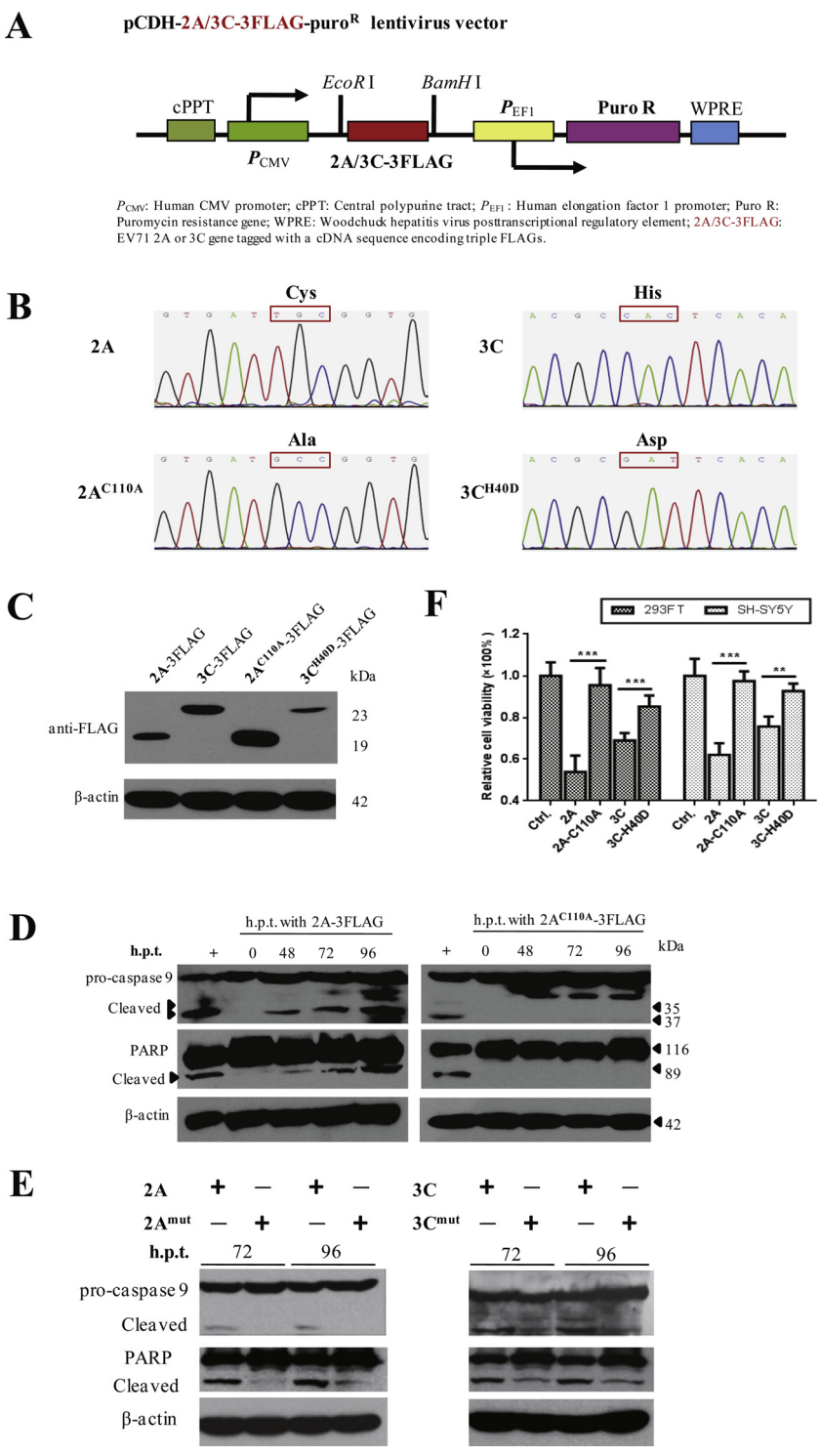

Fig. 6. EV71 2A- and 3C-induced cell death dependent on their protease activity. (A) EV71 2A or 3C gene tagged with a cDNA sequence encoding triple FLAGs was cloned into an overexpressing plasmid pCDH-puro. **(B)** DNA sequencing to identify the construction of EV71 2A, 3C, and their mutants $2A^{C110A}$ and $3C^{H40D}$ with deleted protease activities. **(C)** EV71 2A, 3C, and their mutants expressed in cells after transfection. These plasmids were transfected into 293FT cells for 72 h (3.0 μg/well for each plasmids in a six-well plate), and the cells were collected for immunoblotting. **(D)**. Cleavage of procaspase-9 and PARP in the cells after transfected with EV71 2A plasmids. Plasmid expressing EV71 2A was transfected to 293FT cells at 3.0 μg/well in a six-well plate, and the cells were collected at the indicated time points for immunoblotting. **(E)**. EV71 2A and 3C induced the cleavage of procaspase-9 and PRAP dependent on their protease activity. SH-SY5Y cells were transfected with EV71 2A, 3C, or their protease-deleted mutants at 3.0 μg/well in a six-well plate, and the cells were further incubated for 72 h and 96 h. **(F)**. Cell survival viability was dependent on their protease activity after the cells were transfected with EV71 2A and 3C. These plasmids were transfected (200 ng/well in a 96-well plate) to 293FT or SH-SY5Y cells, and the cells were further incubated for 72 h. Cell survival viability was detected via the MTT assay. Each plasmid transfection was performed in quintuple in the 96-well plate, and the experiment was conducted in triplicate. Data were presented as mean ± SD. $^{**}P < 0.01$ and $^{***}P < 0.001$.

whether the characteristics of EV71-induced cell death is in a similar or in a tissue-specific manner. We observed that EV71 infection mainly induced cell round and shrinkage, but few cells were swollen and ruptured in the two cell lines (Fig. 1A). This finding suggested that the cell death induced by EV71 infection possibly occurred via different pathways. However, most cells infected with EV71 displayed shrinkage (Fig. 1A), nuclear condensation (Fig. 1B), decreased mitochondria potential (Fig. 1C), and disrupted cell membrane and necrosis (Fig. 1D). These findings indicated that most cells underwent apoptosis after they were infected with the virus. Similar results were observed in EV71-infected SF268, SK-N-MC, Vero, Jurkat, and HT-29 cells (Chang et al., 2004; Chen et al., 2006, 2007; Kuo et al., 2002; Li et al., 2002; Lui et al., 2013; Shih et al., 2008).

Some key host factors was subjected to immunoblotting to further identify the molecular events during the virus-induced cell death. The results showed that procaspase-9 and procaspase-3 released their activation forms, and PARP were cleaved after the cells were infected with the virus (Fig. 2). However, activated caspase-8 (data not shown), N-terminal GSDMD, and p-MLKL were not detected in RD, SH-SY5Y, and HeLa cells (Fig. S1). These results implied that the cell death induced by EV71 infection mainly underwent cell apoptosis through the intrinsic pathway rather than GSDMD-mediated pyroptosis and p-MLKL-

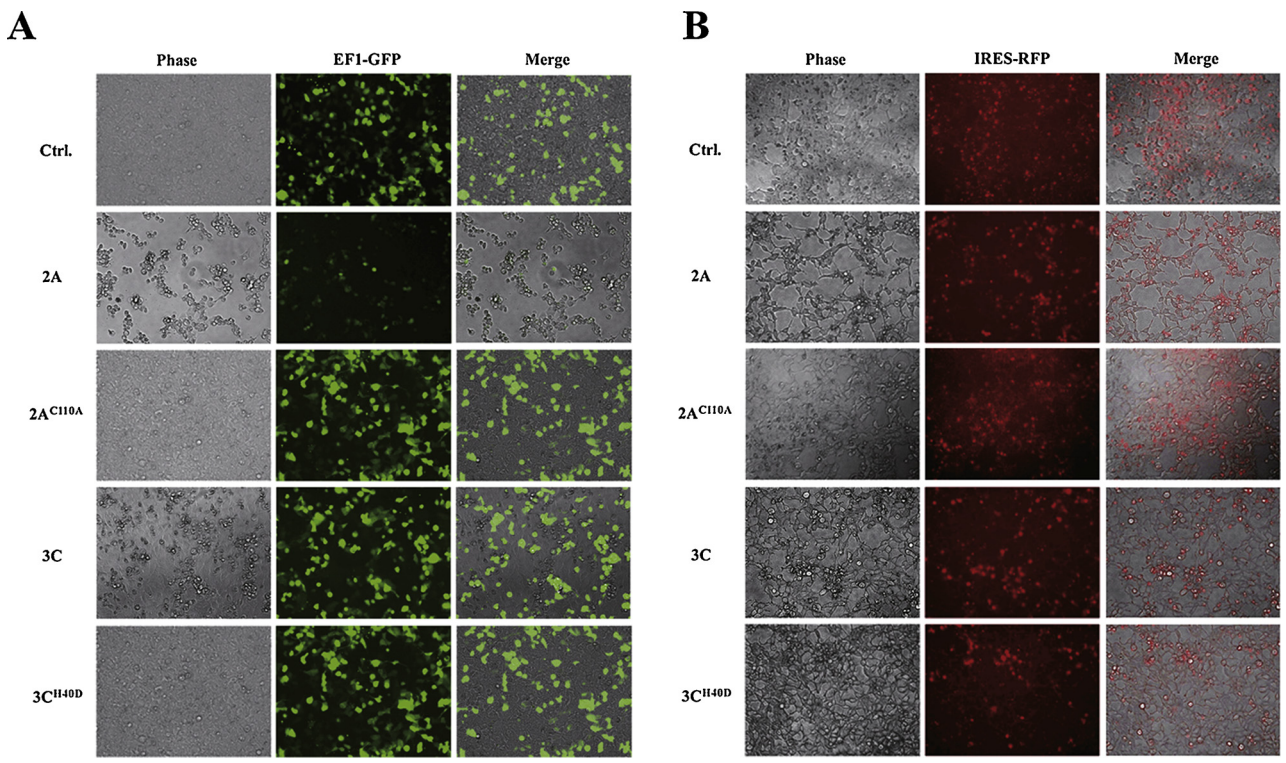

Fig. 7. EV71 2A- and 3C-induced cell death in different mechanisms. (A) EF1α promoter-guided GFP expression evidently inhibited by the co-tranfection with the plasmid expressing EV71 2A but not by $2A^{C110A}$, 3C, or $3C^{H40D}$. EF1α promoter guided-GFP plasmid (500 ng/well) was co-transfected with the given viral protein-expressing constructions (3.0 μg/well for each construction in a six-well plate) in SH-SY5Y cells and incubated for another 72 h. The transfected cells were observed under a microscopy (×200). **(B)** IRES-guided RFP expression was not obviously affected by the co-transfection with EV71 2A, 3C, or their mutants. Transfection was performed as in (A). Each transfection experiment was carried out in triplicate, and the representative results were provided.

mediated necroptosis. After EV71 infection occurred, many PI-staining positive cells and LDH high-release were observed at the late stage of infection (Figs. 1D, 3C, and 3D). Cell death might also be the secondary necrosis of apoptosis instead of GSDMD-mediated pyroptosis or p-MLKL-mediated necroptosis (Fig. S1). Lei et al. (Lei et al., 2017) also described EV71-inhibited cell pyroptosis and observed that EV71 3C cleaves GSDMD at the Q193-G194 pair, resulting in a truncated N-terminal fragment and disrupted function for inducing cell pyroptosis *in vitro*. Whereas Wang et al. (Wang et al., 2015, 2017b), and Yogarajah et al. (Yogarajah et al., 2017) showed that EV71 infection increases AIM-2 expression, activates caspase-1, promotes NLRP3-inflammasome formation, and enhances IL-1β and IL-18 secretion. These observations suggested that EV71 infection can cause cell pyroptosis. These contradictory conclusions might be attributed to various sources of results, including different cell lines *in vitro*, or different tissues *in vivo*, or different infection stages in host. EV71 infection in different cell lines shows a tissue-specific kinetics of viral replication, and the dynamic process is also dependent on the MOIs (Ho et al., 2011; Lin et al., 2009; Lu et al., 2011). However, MOIs do not alter the mechanism of viral infection, including the viral entry, uncoating, replication, and release. Consequently, their different conclusions might not be ascribed to the different MOIs their used. But it is unknown whether the viral strains with different virulence were related to the type of cell death, since different virus strains were utilized by them.

The kinetics of the cells infected with EV71 showed that pretreatment with a pan-caspase inhibitor decreased the number of dead cell, and the amount of released LDH (Fig. 3). The inhibition of virus-induced death by the drug was correlated with the inhibition of procaspase-9 activation, and the cleavage of PARP (Fig. 4), suggesting that EV71-induced cell death is a caspase-dependent process and that apoptosis is the main reason for the virus-induced cell death. However, some cell deaths were still observed even with z-VAD treatment. The phenomena was possibly attributed to the limit of drug concentration not enough to block all caspases under the experiment condition that should not significantly alter the cell viability. Further, it could not exclude that some other unknown caspase-independent pathways might also be activated by the viral infection to induce the infected-cell death. Though the cell death induced by EV71 is mainly by the apoptosis, which is immune-silent, however, there a strong inflammatory response was generally observed in the severe patients (Lin et al., 2003; Wang et al., 2003, 2012). The fact could be ascribed to that there are many triggers in host contributed to the inflammatory response. Besides the virus-induced lytic cell death, the immune response to virus infection also induces many inflammatory cytokines production (Chen et al., 2012; Shih et al., 2011). Further, some signaling pathways, including JNK/MEK, NF-κB, MAPKs, and COX2, could be activated by the virus infection and resulted in strong inflammatory responses (Luo et al., 2017; Peng et al., 2014; Tung et al., 2010).

Though there is a limit by genome scanning to determine the viral genes involved in EV71-induced cell death because the viral genes are always co-expressed in the infected cells and probably form some complexes, whose activities are different from that of the protein or the genomic region expressed alone, the genome scanning would still provide some useful information. Consequently, the genome scanning analysis was performed to identify the genes involved in the virus-induced cell death. The results showed that EV71 2A, 2B, and 3C could be the main contributors of the virus-induced cell death (Fig. 5). EV71 2B is an ion channel protein that induces cell apoptosis by directly modulating the redistribution and activation of the proapoptotic protein BAX (Cong et al., 2016; Han and Cong, 2017). Although the molecular mechanism of EV71 2A- and 3C-induced cell death is largely unknown, the cleavage of the host translation initiation factor 4-gamma 1 (eIF4G1) by 2A (Kuo et al., 2002) and PinX1 (a telomere-binding protein that inhibits the intrinsic telomerase) by 3C (Li et al., 2017)

partially contributes to virus-induced apoptosis. The proteolysis of host proteins by the two viral proteases likely plays an important role in virus-induced cell death. Our experiments confirmed that EV71 2A- and 3C-induced cell death were dependent on their protease activity because the deletion of their protease activity resulted in the loss of their abilities to induce cell death (Fig. 6).

The degradation of eIF4G1 and eIF4E by enteroviruses can shut off host cap-dependent protein translation, whereas viral IRES-dependent translation is unaffected (Ho et al., 2011; Kuo et al., 2002). To test whether EV71 2A- and 3C-induced cell death in a similar way, that is, by shutting off of cellular protein translation with their protease activity, we performed the co-transfection with an EF1α promotor-guided GFP-expressing plasmid with EV71 2A, 3C or their protease activity-deleted mutants. These results indicated that the co-transfection with EV71 2A evidently inhibited the GFP expression but not the co-transfection with $2A^{C110A}$, 3C, and $3C^{H40D}$ (Fig. 7). Considering that EF1α promotor-guided GFP expression is a cap-dependent translation, we deduced that 2A-induced cell death was different from that of 3C-induced cell death, though the two viral proteases were dependent on protease activity. EV71 2A-induced cell death was correlated with the shutoff of host cap-dependent protein translation. However, 3C-induced cell death might be ascribed to the cleavage of other host proteins, which might not to be the key components of translational machinery. The findings also partially explained that the stable cells integrated with 2A-lentivirus could not be available after a drug selection was performed, and 2A in EV71 genome elicited the strongest effects on cell viability after transfection (Figs. 5C, 5D, and 6 F). Further investigation should be performed to identify the specific molecular mechanisms by which the two viral proteases induce cell death.

5. Conclusion

In this study, we identified that EV71-induced cell death mainly involved apoptosis through the intrinsic pathway. Cell death after EV71 infection was possibly triggered by viral 2A, 2B, or 3C. Cell death induced by 2A and 3C was dependent on their protease activity. EV71 2A-induced cell death possibly occurred through the shutoff of host protein translation, but 3C-induced cell death might not be the case.

Disclosures

The authors declare no conflict of interest with respect to the publication of this paper.

Acknowledgments

This work was supported by the National Natural Science Foundation of China (NSFC. 31570156) and partially funded by the National Science and Technology Major Project on Infectious Diseases (2012ZX10004503-003).

Appendix A. Supplementary data

Supplementary material related to this article can be found, in the online version, at doi:https://doi.org/10.1016/j.virusres.2019.03.017.

References

Adeyemi, O.O., Sherry, L., Ward, J.C., Pierce, D.M., Herod, M.R., Rowlands, D.J., Stonehouse, N.J., 2018. Involvement of a non-structural protein in poliovirus capsid assembly. J. Virol. https://doi.org/10.1128/JVI.01447-18.

Bek, E.J., McMinn, P.C., 2012. The pathogenesis and prevention of encephalitis due to human enterovirus 71. Curr. Infect. Dis. Rep. 14 (4), 397–407.

Bian, L., Wang, Y., Liu, Q., Xia, J., Long, J.E., 2015. Prediction of signaling pathways involved in enterovirus 71 infection by algorithm analysis based on miRNA profiles and their target genes. Arch. Virol. 160 (1), 173–182.

Cai, Z., Jitkaew, S., Zhao, J., Chiang, H.C., Choksi, S., Liu, J., Ward, Y., Wu, L.G., Liu, Z.G., 2014. Plasma membrane translocation of trimerized MLKL protein is required for TNF-induced necroptosis. Nat. Cell Biol. 16 (1), 55–65.

Chan, F.K., Luz, N.F., Moriwaki, K., 2015. Programmed necrosis in the cross talk of cell death and inflammation. Annu. Rev. Immunol. 33, 79–106.

Chang, S.C., Lin, J.Y., Lo, L.Y., Li, M.L., Shih, S.R., 2004. Diverse apoptotic pathways in enterovirus 71-infected cells. J. Neurovirol. 10 (6), 338–349.

Chen, L.C., Shyu, H.W., Chen, S.H., Lei, H.Y., Yu, C.K., Yeh, T.M., 2006. Enterovirus 71 infection induces Fas ligand expression and apoptosis of Jurkat cells. J. Med. Virol. 78 (6), 780–786.

Chen, T.C., Lai, Y.K., Yu, C.K., Juang, J.L., 2007. Enterovirus 71 triggering of neuronal apoptosis through activation of Abl-Cdk5 signalling. Cell. Microbiol. 9 (11), 2676–2688.

Chen, J., Tong, J., Liu, H., Liu, Y., Su, Z., Wang, S., Shi, Y., Zheng, D., Sandoghchian, S., Geng, J., Xu, H., 2012. Increased frequency of Th17 cells in the peripheral blood of children infected with enterovirus 71. J. Med. Virol. 84 (5), 763–767.

Cong, H., Du, N., Yang, Y., Song, L., Zhang, W., Tien, P., 2016. Enterovirus 71 2B induces cell apoptosis by directly inducing the conformational activation of the proapoptotic protein bax. J. Virol. 90 (21), 9862–9877.

Cui, S., Wang, J., Fan, T., Qin, B., Guo, L., Lei, X., Wang, J., Wang, M., Jin, Q., 2011. Crystal structure of human enterovirus 71 3C protease. J. Mol. Biol. 408 (3), 449–461.

Ding, J., Wang, K., Liu, W., She, Y., Sun, Q., Shi, J., Sun, H., Wang, D.C., Shao, F., 2016. Pore-forming activity and structural autoinhibition of the gasdermin family. Nature 535 (7610), 111–116.

Eray, M., Matto, M., Kaartinen, M., Andersson, L.C., Pelkonen, J., 2001. Flow cytometric analysis of apoptotic subpopulations with a combination of annexin V-FITC, propidium iodide, and SYTO 17. Cytometry 43 (2), 134–142.

Fung, G., Shi, J., Deng, H., Hou, J., Wang, C., Hong, A., Zhang, J., Jia, W., Luo, H., 2015. Cytoplasmic translocation, aggregation, and cleavage of TDP-43 by enteroviral proteases modulate viral pathogenesis. Cell Death Differ. 22 (12), 2087–2097.

Han, X., Cong, H., 2017. Enterovirus 71 induces apoptosis by directly modulating the conformational activation of pro-apoptotic protein Bax. J. Gen. Virol. 98 (3), 422–434.

Ho, B.C., Yu, S.L., Chen, J.J., Chang, S.Y., Yan, B.S., Hong, Q.S., Singh, S., Kao, C.L., Chen, H.Y., Su, K.Y., Li, K.C., Cheng, C.L., Cheng, H.W., Lee, J.Y., Lee, C.N., Yang, P.C., 2011. Enterovirus-induced miR-141 contributes to shutoff of host protein translation by targeting the translation initiation factor eIF4E. Cell Host Microbe 9 (1), 58–69.

Huang, M.L., Camara, A.K.S., Stowe, D.F., Beard, D.A., 2007. Quantitative analysis of mitochondrial membrane potential measurements with JC-1. Faseb J. 21 (6) A1351-A1351.

Kaczmarek, A., Vandenabeele, P., Krysko, D.V., 2013. Necroptosis: the release of damage-associated molecular patterns and its physiological relevance. Immunity 38 (2), 209–223.

Kaiser, W.J., Upton, J.W., Mocarski, E.S., 2013. Viral modulation of programmed necrosis. Curr. Opin. Virol. 3 (3), 296–306.

Kovacs, S.B., Miao, E.A., 2017. Gasdermins: effectors of pyroptosis. Trends Cell Biol. 27 (9), 673–684.

Kuo, R.L., Kung, S.H., Hsu, Y.Y., Liu, W.T., 2002. Infection with enterovirus 71 or expression of its 2A protease induces apoptotic cell death. J. Gen. Virol. 83 (Pt 6), 1367–1376.

Lee, K.Y., 2016. Enterovirus 71 infection and neurological complications. Korean J. Pediatr. 59 (10), 395–401.

Lei, X., Zhang, Z., Xiao, X., Qi, J., He, B., Wang, J., 2017. Enterovirus 71 inhibits pyroptosis through cleavage of GSDMD. J. Virol.

Li, M.L., Hsu, T.A., Chen, T.C., Chang, S.C., Lee, J.C., Chen, C.C., Stollar, V., Shih, S.R., 2002. The 3C protease activity of enterovirus 71 induces human neural cell apoptosis. Virology 293 (2), 386–395.

Li, J., Yao, Y., Chen, Y., Xu, X., Lin, Y., Yang, Z., Qiao, W., Tan, J., 2017. Enterovirus 71 3C promotes apoptosis through cleavage of PinX1, a telomere binding protein. J. Virol. 91 (2).

Lin, T.Y., Hsia, S.H., Huang, Y.C., Wu, C.T., Chang, L.Y., 2003. Proinflammatory cytokine reactions in enterovirus 71 infections of the central nervous system. Clin. Infect. Dis. 36 (3), 269–274.

Lin, Y.W., Wang, S.W., Tung, Y.Y., Chen, S.H., 2009. Enterovirus 71 infection of human dendritic cells. Exp. Biol. Med. (Maywood) 234 (10), 1166–1173.

Lu, J., He, Y.Q., Yi, L.N., Zan, H., Kung, H.F., He, M.L., 2011. Viral kinetics of enterovirus 71 in human abdomyosarcoma cells. World J. Gastroenterol. 17 (36), 4135–4142.

Lui, Y.L.E., Timms, P., Hafner, L.M., Tan, T.L., Tan, K.H., Tan, E.L., 2013. Characterisation of enterovirus 71 replication kinetics in human colorectal cell line, HT29. Springerplus 2.

Luo, Z., Ge, M., Chen, J., Geng, Q., Tian, M., Qiao, Z., Bai, L., Zhang, Q., Zhu, C., Xiong, Y., Wu, K., Liu, F., Liu, Y., Wu, J., 2017. HRS plays an important role for TLR7 signaling to orchestrate inflammation and innate immunity upon EV71 infection. PLoS Pathog. 13 (8), e1006585.

Lupfer, C., Malik, A., Kanneganti, T.D., 2015. Inflammasome control of viral infection. Curr. Opin. Virol. 12, 38–46.

McMinn, P.C., 2012. Recent advances in the molecular epidemiology and control of human enterovirus 71 infection. Curr. Opin. Virol. 2 (2), 199–205.

Mu, Z., Wang, B., Zhang, X., Gao, X., Qin, B., Zhao, Z., Cui, S., 2013. Crystal structure of 2A proteinase from hand, foot and mouth disease virus. J. Mol. Biol. 425 (22), 4530–4543.

Murphy, J.M., Czabotar, P.E., Hildebrand, J.M., Lucet, I.S., Zhang, J.G., Alvarez-Diaz, S., Lewis, R., Lalaoui, N., Metcalf, D., Webb, A.I., Young, S.N., Varghese, L.N., Tannahill, G.M., Hatchell, E.C., Majewski, I.J., Okamoto, T., Dobson, R.C., Hilton, D.J., Babon, J.J., Nicola, N.A., Strasser, A., Silke, J., Alexander, W.S., 2013. The pseudokinase MLKL mediates necroptosis via a molecular switch mechanism. Immunity 39 (3), 443–453.

Nagata, S., Tanaka, M., 2017. Programmed cell death and the immune system. Nat. Rev. Immunol. 17 (5), 333–340.
Oliver, F.J., de la Rubia, G., Rolli, V., Ruiz-Ruiz, M.C., de Murcia, G., Menissier-de Murcia, J., 1998. Importance of poly(ADP-ribose) polymerase and its cleavage in apoptosis - Lesson from an uncleavable mutant. J. Biol. Chem. 273 (50), 33533–33539.
Ong, K.C., Wong, K.T., 2015. Understanding enterovirus 71 neuropathogenesis and its impact on other neurotropic enteroviruses. Brain Pathol. 25 (5), 614–624.
Ooi, M.H., Wong, S.C., Lewthwaite, P., Cardosa, M.J., Solomon, T., 2010. Clinical features, diagnosis, and management of enterovirus 71. Lancet Neurol. 9 (11), 1097–1105.
Orzalli, M.H., Kagan, J.C., 2017. Apoptosis and Necroptosis as host defense strategies to prevent viral infection. Trends Cell Biol.
Pasparakis, M., Vandenabeele, P., 2015. Necroptosis and its role in inflammation. Nature 517 (7534), 311–320.
Pathinayake, P.S., Hsu, A.C., Wark, P.A., 2015. Innate immunity and immune evasion by enterovirus 71. Viruses 7 (12), 6613–6630.
Peng, H., Shi, M., Zhang, L., Li, Y., Sun, J., Zhang, L., Wang, X., Xu, X., Zhang, X., Mao, Y., Ji, Y., Jiang, J., Shi, W., 2014. Activation of JNK1/2 and p38 MAPK signaling pathways promotes enterovirus 71 infection in immature dendritic cells. BMC Microbiol. 14, 147.
Place, D.E., Kanneganti, T.D., 2017. Recent advances in inflammasome biology. Curr. Opin. Immunol. 50, 32–38.
Shi, J., Zhao, Y., Wang, K., Shi, X., Wang, Y., Huang, H., Zhuang, Y., Cai, T., Wang, F., Shao, F., 2015. Cleavage of GSDMD by inflammatory caspases determines pyroptotic cell death. Nature 526 (7575), 660–665.
Shi, J.J., Gao, W.Q., Shao, F., 2017. Pyroptosis: gasdermin-mediated programmed necrotic cell death. Trends Biochem. Sci. 42 (4), 245–254.
Shih, S.R., Weng, K.F., Stollar, V., Li, M.L., 2008. Viral protein synthesis is required for Enterovirus 71 to induce apoptosis in human glioblastoma cells. J. Neurovirol. 14 (1), 53–61.
Shih, S.R., Stollar, V., Li, M.L., 2011. Host factors in enterovirus 71 replication. J. Virol. 85 (19), 9658–9666.
Solomon, T., Lewthwaite, P., Perera, D., Cardosa, M.J., McMinn, P., Ooi, M.H., 2010. Virology, epidemiology, pathogenesis, and control of enterovirus 71. Lancet Infect. Dis. 10 (11), 778–790.
Tung, W.H., Hsieh, H.L., Yang, C.M., 2010. Enterovirus 71 induces COX-2 expression via MAPKs, NF-kappaB, and AP-1 in SK-N-SH cells: role of PGE(2) in viral replication. Cell. Signal. 22 (2), 234–246.
Wang, S.M., Lei, H.Y., Huang, K.J., Wu, J.M., Wang, J.R., Yu, C.K., Su, I.J., Liu, C.C., 2003. Pathogenesis of enterovirus 71 brainstem encephalitis in pediatric patients: roles of cytokines and cellular immune activation in patients with pulmonary edema. J. Infect. Dis. 188 (4), 564–570.
Wang, S.M., Lei, H.Y., Liu, C.C., 2012. Cytokine immunopathogenesis of enterovirus 71 brain stem encephalitis. Clin. Dev. Immunol. 2012, 876241.
Wang, H., Lei, X., Xiao, X., Yang, C., Lu, W., Huang, Z., Leng, Q., Jin, Q., He, B., Meng, G., Wang, J., 2015. Reciprocal regulation between enterovirus 71 and the NLRP3 inflammasome. Cell Rep. 12 (1), 42–48.
Wang, T., Wang, B., Huang, H., Zhang, C.Y., Zhu, Y.M., Pei, B., Cheng, C.F., Sun, L., Wang, J.W., Jin, Q., Zhao, Z.D., 2017a. Enterovirus 71 protease 2A(pro) and 3C(pro) differentially inhibit the cellular endoplasmic reticulum-associated degradation (ERAD) pathway via distinct mechanisms, and enterovirus 71 hijacks ERAD component p97 to promote its replication. PLoS Pathog. 13 (10).
Wang, W., Xiao, F., Wan, P., Pan, P., Zhang, Y., Liu, F., Wu, K., Liu, Y., Wu, J., 2017b. EV71 3D protein binds with NLRP3 and enhances the assembly of inflammasome complex. PLoS Pathog. 13 (1), e1006123.
Wang, Y., Qin, Y., Wang, T.Y., Chen, Y., Lang, X.J., Zheng, J., Gao, S.Y., Chen, S.J., Zhong, X.Y., Mu, Y.S., Wu, X.Y., Zhang, F.M., Zhao, W.R., Zhong, Z.H., 2018. Pyroptosis induced by enterovirus 71 and coxsackievirus B3 infection affects viral replication and host response. Sci. Rep. 8.
Weng, K.F., Chen, L.L., Huang, P.N., Shih, S.R., 2010. Neural pathogenesis of enterovirus 71 infection. Microbes Infect. 12 (7), 505–510.
Xing, W., Liao, Q., Viboud, C., Zhang, J., Sun, J., Wu, J.T., Chang, Z., Liu, F., Fang, V.J., Zheng, Y., Cowling, B.J., Varma, J.K., Farrar, J.J., Leung, G.M., Yu, H., 2014. Hand, foot, and mouth disease in China, 2008–12: an epidemiological study. Lancet Infect. Dis. 14 (4), 308–318.
Yan, X.F., Gao, S., Xia, J.F., Ye, R., Yu, H., Long, J.E., 2012. Epidemic characteristics of hand, foot, and mouth disease in Shanghai from 2009 to 2010: enterovirus 71 subgenotype C4 as the primary causative agent and a high incidence of mixed infections with coxsackievirus A16. Scand. J. Infect. Dis. 44 (4), 297–305.
Yang, X.D., Hu, Z.L., Fan, S.S., Zhang, Q., Zhong, Y., Guo, D., Qin, Y.L., Chen, M.Z., 2018. Picornavirus 2A protease regulates stress granule formation to facilitate viral translation. PLoS Pathog. 14 (2).
Yogarajah, T., Ong, K.C., Perera, D., Wong, K.T., 2017. AIM2 inflammasome-mediated pyroptosis in enterovirus A71-Infected neuronal cells restricts viral replication. Sci. Rep. 7 (1), 5845.
Yuan, J., Shen, L., Wu, J., Zou, X., Gu, J., Chen, J., Mao, L., 2018. Enterovirus A71 proteins: structure and function. Front. Microbiol. 9, 286.